Chapter 13

Inverse Raman Scattering in Femtosecond Broadband Transient Absorption Experiments

Antonio Aloi and Raffaele Tommasi

Additional information is available at the end of the chapter

http://dx.doi.org/10.5772/65479

Abstract

This chapter reports on one of the nonlinear spectral features, the inverse Raman scattering (IRS), observed upon the interaction of ultrafast-pulsed lasers in a Raman-active medium. Hereby, a comprehensive theoretical description of the IRS is exposed. Furthermore, the investigation carried out on synthetic eumelanin dispersions is addressed to show how the transient absorption measurements can be influenced by the IRS, if probing at energies close to Stokes and anti-Stokes vibrational modes of the medium. A thorough analysis demonstrates that the IRS affects the sign of dynamics but not relaxation times. A specific kind of spectroscopy based on the IRS effect (ultrafast Raman loss spectroscopy) is eventually illustrated as valuable tool to characterize the structure of molecules and to investigate their dynamics during chemical reactions, even occurring at ultrafast timescales.

Keywords: nonlinear Raman spectroscopy, stimulated Raman scattering, inverse Raman-scattering, femtosecond transient absorption spectroscopy, stimulated Raman gain spectroscopy (SRGS), ultrafast Raman loss spectroscopy (URLS)

1. Introduction

Nowadays, the possibility to investigate optical nonlinearities offers great insights on material properties and the interaction between light and matter. After the interaction with a strong optical field, the response of the material will be no longer linearly dependent on its strength, instead nonlinear effects start playing major roles. Due to crystal structures and symmetries of media, the third order is the nonlinearity of the lowest order that can be observed in all media [1], and thus has become a valuable tool to investigate structural and dynamic aspects

of matter. Among the third-order nonlinear effects (e.g., third-harmonic generation, optical Kerr effect), the four-wave mixing (FWM) is the mostly explored since it generalizes all the third-order nonlinearities. The FWM relies on the mixing of three input signals, which results in the generation of a fourth output field. When one of the input signals is resonant with the frequencies of the material, the FWM process can be enhanced and is called *stimulated Raman scattering* (SRS). Coupling this process with laser pulses delayed in time, namely using a pump-probe setup, it is possible to investigate the temporal behavior of the material and the evolution of its properties. Nonlinear Raman spectroscopy is an example of such combination between third-order nonlinear optical effect and pump-probe technique [2].

In this chapter, we discuss one of the FWM processes which contributes to the stimulated Raman scattering, called inverse Raman scattering (IRS). The theory behind the IRS effect will be explained, resorting to Feynman dual-time line (FDTL) diagrams [3], as well as its application as a spectroscopic tool. Furthermore, the connection held between the IRS and the femtosecond transient absorption (FTA) spectroscopy will be clarified, pointing out the important role the IRS effect plays on the temporal evolution of relaxation dynamics in FTA.

2. Inverse Raman scattering: theory

To describe the SRS and its origin, we begin by discussing the interaction of an optical field of frequency ω_L with a Raman-active medium, restricted to the scalar approximation. A vibrational mode in a Raman-active medium can be described as a simple harmonic oscillator with frequency ω_v. Due to vibrations, the optical polarizability of the molecules will change in time, depending on their reciprocal distance (internuclear separation). The periodic variation of the molecule polarizability will generate a modulation in the refractive index, which in turn will modify an incoming light beam of frequency ω_L. Specifically, the frequencies $\omega_L \pm \omega_v$ will be superimposed upon the transmitted light beam. The stimulated Raman scattering can be visually understood in terms of the interactions shown in **Figure 1**. **Figure 1a**

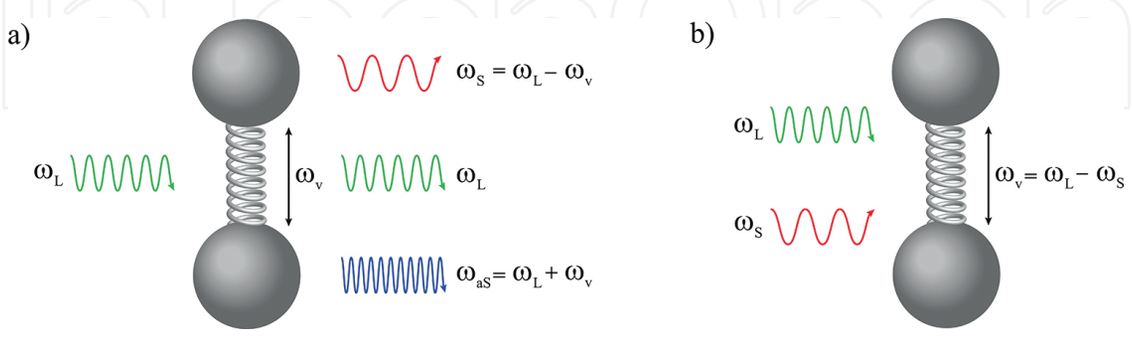

Figure 1. Schematic showing the stimulated Raman-scattering process. The molecules in the Raman-active medium are described by harmonic oscillators of frequency ω_v. The incoming laser beam has frequency ω_L. (a) Modulation of the refractive index and subsequent emission of Stokes and anti-Stokes radiation and (b) beating of the Stokes frequency with the laser field reinforcing the vibrational oscillation of the molecule.

http://dx.doi.org/10.5772/65479

shows the modulation of the refractive index due to the vibrational frequencies of the medium, thereby the transmitted light will carry the Stokes ($\omega_S = \omega_L - \omega_v$) and anti-Stokes ($\omega_{aS} = \omega_L + \omega_v$) frequencies besides the laser frequency ω_L. At the same time, one of the newly generated frequencies can beat with the incoming laser beam frequency, modulating the amplitude of the molecular vibrations (**Figure 1b**).

The two processes hereby depicted reinforce one another: the modulation of the vibrational frequencies interacts with the incoming laser beam frequency, leading to a Stokes field which increases the amplitude of the vibrational oscillation, and eventually strengthens the Stokes frequencies. This condition of amplification is called vibrational coherence, and it can be probed by a third laser beam, determining the stimulated Raman scattering [4]. The mathematical expressions of energy conservation and phase matching are given below:

$$\begin{aligned} \omega_{\mathrm{SRS}} &= \left(\omega_L - \omega_S\right) \pm \omega_L = \omega_v \pm \omega_L \\ \boldsymbol{k}_{\mathrm{SRS}} &= \left(\boldsymbol{k}_L - \boldsymbol{k}_S\right) \pm \boldsymbol{k}_L = \boldsymbol{k}_v \pm \boldsymbol{k}_L \end{aligned} \tag{1}$$

with ω_{SRS} and $\boldsymbol{k}_{\mathrm{SRS}}$ the frequency and the wave vector of the SRS signal, respectively. If the incoming optical field is a femtosecond pulse, and the probing beam is a broadband white-light continuum (WLC), then the process is called *femtosecond stimulated Raman scattering* (FSRS), and is one of the four-wave-mixing processes. Among all the possible interactions of the fields involved, these can be narrowed down to two main terms called stimulated Raman scattering, and inverse Raman scattering [2]. Hereby, we focus on the inverse Raman-scattering effect.

The probability of annihilation of a photon with frequency ω_L and the simultaneous creation of another photon with frequency $\omega_1 = \omega_L \pm \omega_v$, according to the Kramers-Heisenberg dispersion formula, is given by [5]

$$P = \frac{16\pi^4}{h^4} \int |\mu|^2 \rho_0 \left(\rho_1 + \frac{8\pi h \omega_1^3}{c^3} \right) d\omega_0, \tag{2}$$

where μ is the probability of the two-photon process, $\rho_0 \rho_1$ is associated to the IRS process, while $\rho_0 8\pi h \omega_1^3$ takes into account the spontaneous Raman scattering. A generalization of Eq. (2) was proposed by Mukamel to describe the stimulated Raman-scattering signal as [6]

$$\begin{aligned}\tilde{S}_{SRS}\left(\omega_{pu},\omega_{pr}\right) = 4\pi N \sum_{g,g',e,f} & P(g)\left|\varepsilon_{pu}\right|^2\left|\varepsilon_{pr}\right|^2\left|T^{(2)}_{g'g}\left(\omega_{pu}\right)\right|^2\delta\left(\omega_{pu}-\omega_{pr}-\omega_{g'g}\right)\\ & - P(g)\left|\varepsilon_{pu}\right|^2\left|\varepsilon_{pr}\right|^2\left|T^{(2)}_{g'g}\left(\omega_{pr}\right)\right|^2\delta\left(\omega_{pr}-\omega_{pu}-\omega_{g'g}\right)\\ & + P(g)\left|\varepsilon_{pr}\right|^2\left|T^{(1)}_{eg}\right|^2\delta\left(\omega_{pr}-\omega_{eg}\right)\\ & - P(g)\left|\varepsilon_{pr}T^{(1)}_{eg}+\left|\varepsilon_{pu}\right|^2\varepsilon_{pr}T^{(3)}_{eg}\left(\omega_{pr}-\omega_{pu},\omega_{pr}\right)\right|^2\\ & + \left|\varepsilon_{pu}\right|^2\varepsilon_{pr}T^{(3)}_{eg}\left(\omega_{pr}-\omega_{pu},\omega_{pu}\right)\delta\left(\omega_{pr}-\omega_{eg}\right).\end{aligned} \tag{3}$$

Here, N is the number of molecules involved in the scattering process, $\varepsilon_{\mathrm{pu}}$ ($\varepsilon_{\mathrm{pr}}$) and ω_{pu} (ω_{pr}) are the amplitudes and frequencies, respectively, of the pump (probe) field. $P(g)$ indicates the ground-state population at equilibrium $|g\rangle$, while $T^{(1)}_{\mathrm{eg}}$ is a matrix defining the scattering process, showing the order of the transition ($i = 2$ two-photon process, $i = 3$ three-photon process, etc.), and the initial and final states involved. Eq. (3) can be explained as follows: the first term describes the loss of a photon with frequency ω_{pu}, and the emission of a photon (gain process) with frequency ω_{pr}. Conversely, the second term takes into account the emission of a pump-beam photon after the annihilation of a photon of the probe beam (loss process). Both third and fourth terms describe the perturbation in the probe-field absorption due to the coexistence of the pump field [7].

As stated in Eq. (3), the absorption of a photon with frequency ω_{pu}, or the emission at frequency ω_1, depends on the population of the states involved in the transition, and specifically on the ratio between the number of molecules in the excited vibrational state and the number of molecules in the ground state. At room temperature, the excited states are scarcely populated; hence, a radiation is most likely emitted at Stokes frequencies, while absorbed at anti-Stokes frequencies [8].

Even if there are other nonlinear processes involved, due to the intensity of the laser field typically used, the treatment of the SRS can be narrowed down to three relevant equations in the classical description, reporting on the laser excitation frequency ω_{pu}, and the Stokes and anti-Stokes frequencies ω_S, ω_{aS}:

$$\frac{dA_m\left(\omega_{pu}\right)}{dz} = \frac{2\pi i\omega_{pu}}{n_{pu}c}\chi_{mjkl}A_j\left(\omega_S\right)A_k\left(\omega_{aS}\right)A^*_l\left(\omega_{pu}\right)e^{-i\Delta kz} + \sum_{\mu=L,S,aS}\chi_{mjkl}A_j\left(\omega_{pu}\right)A_k\left(\omega_\mu\right)A^*_l\left(\omega_\mu\right), \tag{4}$$

$$\frac{dA_k\left(\omega_S\right)}{dz} = \frac{2\pi i\omega_S}{n_Sc}\chi_{kjml}A_j\left(\omega_{pu}\right)A^*_m\left(\omega_{aS}\right)A_l\left(\omega_{pu}\right)e^{i\Delta kz} + \sum_{\mu=L,aS,S}\chi_{klmn}A_l\left(\omega_S\right)A_m\left(\omega_\mu\right)A^*_n\left(\omega_\mu\right), \tag{5}$$

http://dx.doi.org/10.5772/65479

$$\frac{dA_j^*(\omega_{aS})}{dz} = -\frac{2\pi i\omega_{aS}}{n_{aS}c}\chi_{jklm}A_k^*(\omega_{pu})A_l(\omega_S)A_m^*(\omega_{pu})e^{-i\Delta kz} + \sum_{\mu=L,aS,S}\chi_{jklm}A_k^*(\omega_{aS})A_l(\omega_\mu)A_m^*(\omega_\mu). \quad (6)$$

Here, χ_{mjkl} are the nonlinear susceptibilities at the interacting frequencies, while n is the refractive index modulated by the fields at their specific frequency. The wave vectors are related to one another by the phase-matching condition $\Delta\boldsymbol{k} = 2\boldsymbol{k}_{\mathrm{pu}} - \boldsymbol{k}_S - \boldsymbol{k}_{aS} = 0$. On one hand, the real part of the susceptibility describes the refractive index modulation due to the incoming field, and thus expresses the phase modulation. The imaginary part, on the other hand, accounts for the nonlinear Raman scattering and the two-photon absorption. Resorting to Eqs. (4)–(6), it is possible to describe all the processes involved in the SRS effect. The equations needed to describe the IRS effect alone are fewer, though. To simplify the theoretical treatment, few assumptions can be done without loss of generality. In fact, it can be expected that the incoming light intensity is stronger than the scattered one, that is, $I_{\mathrm{pu}} \gg I_S,\quad I_{aS}$. Furthermore, the intensity of the IRS is stronger than the spontaneous Raman scattering if detected at the same frequency. Thus, in the scalar approximation for the susceptibility, Eqs. (4)–(6) can be rewritten as

$$\frac{dA_s}{dz} = \frac{2\pi i\omega_S}{n_S c}\left(\chi\left|A_{pu}\right|^2 A_S + \chi A_{pu}^* A_{aS}^* e^{i\Delta kz}\right), \quad (7)$$

$$\frac{dA_{as}}{dz} = -\frac{2\pi i\omega_{aS}}{n_{aS}c}\left(\chi A_{pu}^* A_S^* e^{-i\Delta kz} + \chi\left|A_{pu}\right|^2 A_{aS}^*\right), \quad (8)$$

assuming that the incoming field intensity is constant, that is, $dA_{\mathrm{pu}}/dz = 0$. It follows that the intensities of the Stokes and anti-Stokes fields are

$$I_S(z) = r_1^2\exp\left(2|g|I_{pu}z\right) + r_2^2\exp\left(-2|g|I_{pu}z\right) + 2r_1r_2\cos\left(\Delta kz + \delta\phi\right), \quad (9)$$

$$I_{aS}(z) = \alpha_1 r_1^2\exp\left(2|g|I_{pu}z\right) + \alpha_2 r_2^2\exp\left(-2|g|I_{pu}z\right) - 2r_1r_2\cos\left(\Delta kz + \delta\phi\right). \quad (10)$$

where $g = (2\pi\omega/nc)\Im\chi$. The terms r_i and α_i are defined by the initial conditions, and specifically $\alpha_1 \le 1,\quad \alpha_2 \ge 1$; $\delta\phi$ is the initial phase shift at the front of the sample. Depending on the ratio $gI_{\mathrm{pu}}/\Delta k$ and hence on the Stokes-anti-Stokes coupling, three different solutions to the system can be found [8]. Here, the solution for zero coupling ($gI_{\mathrm{pu}} < \Delta k$) will be presented, due to the noncollinear geometry of the pump-probe setup (for the other solutions, refer to

Weigmann's paper [8]). The condition hereby described predicts an enhancement of the IRS signal, with the intensities at the Stokes and anti-Stokes frequencies given by

$$I_S(z) \simeq r_1^2 \exp\left(2|g| I_{pu} z\right), \tag{11}$$

$$I_{aS}(z) \simeq \alpha_2 r_2^2 \exp\left(-2|g| I_{pu} z\right). \tag{12}$$

It follows that the intensities at the anti-Stokes frequencies are higher than the corresponding ones at the Stokes frequencies [7, 9, 10]. In the spontaneous Raman scattering, at room temperature the populations in the excited vibrational levels are negligible, as described by Boltzmann distribution, thus the anti-Stokes peaks are weak. However, in the stimulated process (such as IRS) the Boltzmann distribution does not describe anymore the energy levels population, and a strong anti-Stokes emission can be observed [11].

3. Inverse Raman scattering: spectroscopy

The IRS effect can be described by the Feynman dual-time line (FDTL) diagrams in the Liouville space with the ket and bra evolution (**Figure 2**) [12]. Using the FDTL diagrams and the related energy level diagrams, it is possible to illustrate the temporal evolution of the density matrix in the four-wave mixing process, which the IRS is based on. The temporal evolution goes from τ_3 to t when the third-order polarization induced in the medium is computed [3]. The arrows pointing into the time line represent the absorption from the ground state $\left|\Psi_{g0}\right\rangle$ to the excited state $\left|\Psi_{e}\right\rangle$ and the related wave vector is $+\mathbf{k}$ On the contrary, the arrows pointing far from the time line illustrate the stimulated emission from $\left|\Psi_{e}\right\rangle$ to $\left|\Psi_{g0}\right\rangle$ and their wave vector is $-\mathbf{k}$.

In the energy diagrams, $\boldsymbol{E}_{\mathrm{pr}}$, $\boldsymbol{E}_{\mathrm{pu}}$, and $\boldsymbol{E}^*_{\mathrm{pu}}$ are the vectors of the fields involved in the interaction in the medium, having frequencies ω_{pr}, $\omega_{\mathrm{pu,}}$ and ω_{pu} respectively. In both IRS (I) and IRS (II) processes, the wave vectors of the incoming pump fields, that is, $\boldsymbol{k}_{\mathrm{pu}}$ and $\boldsymbol{k}^*_{\mathrm{pu}}$, vanish, leading to a third-order polarization having the same direction of the incoming pump pulse [12]. The difference between the IRS (I) and IRS (II) lays in the sequence with which pump and probe pulses reach the sample. In the IRS (I) (**Figure 2a**), the excitation process is started by the probe pulse alone at frequencies higher than those of pump pulse, that is, in the anti-Stokes region. The vibrational coherence persists as long as the pump pulse overlaps with the probe pulse, then a photon with frequency ω_{pr} is annihilated due to the interaction between the two pulses, and a loss in intensity in the probe spectrum is observed at the specified anti-Stokes frequency [13]. In the IRS (II) (**Figure 2b**), the pump pulse is followed by the probe pulse, it induces the excitation in the sample and due to the interaction of the two fields, the vibrational coherence is achieved. A photon having frequency ω_{pr} and wave vector $\boldsymbol{k_S}$ (i.e., same direction of the

http://dx.doi.org/10.5772/65479

Stokes radiation) is created, and it adds to the probe pulse, leading to an intensity gain in the probe spectrum at the specified frequency. According to the energy conservation, a loss in energy, equal to the gain obtained at the Stokes frequency, is observed in the pump pulse [4]. This is clearly shown in the bottom part of **Figure 2a** and **2b**, where the frequency of the outcoming beam is higher (lower) than the one of the pump fields for the anti-Stokes (Stokes) signal.

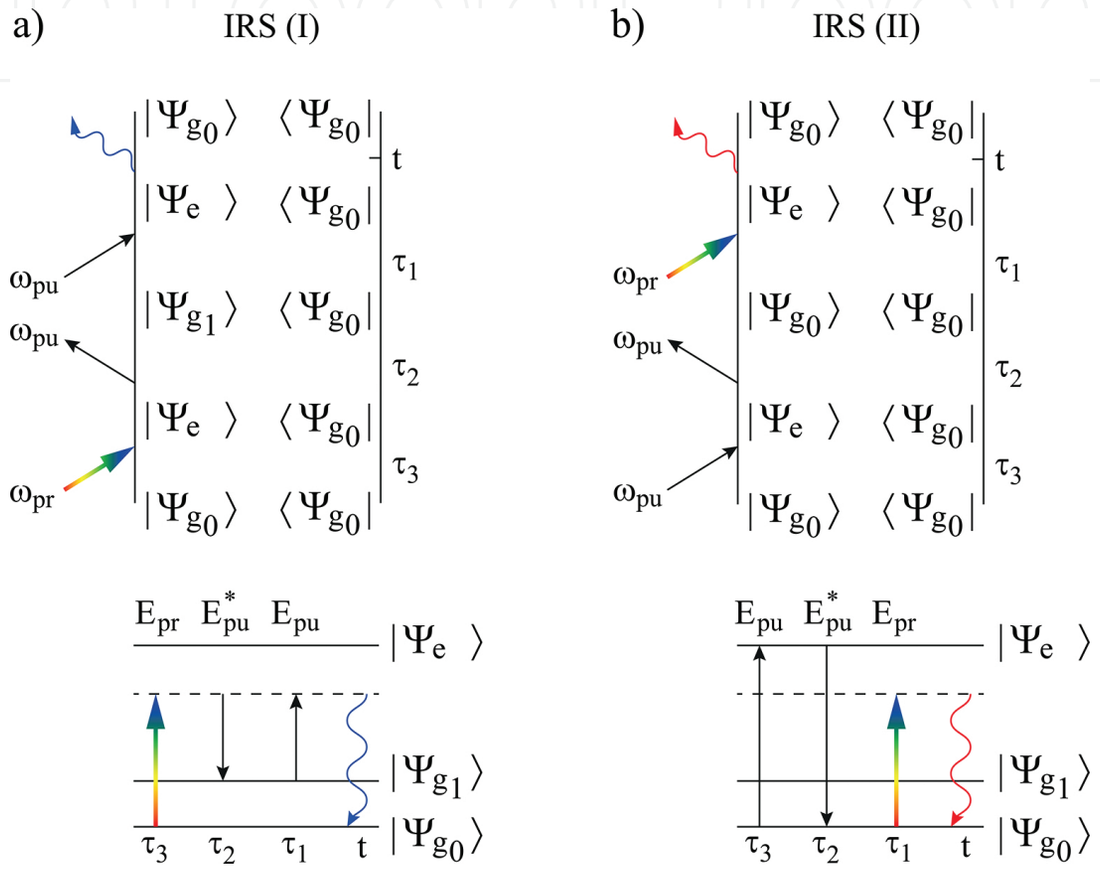

Figure 2. Feynman dual-time line (FDTL) diagrams (top) and energy-level diagrams (bottom) describing the IRS effect. The wavy line is the field coming out from the stimulated Raman-scattering process, and illustrates the third-order polarization of the involved energetic states. In the energy diagrams, the solid and the dashed lines represent the real and the virtual levels, respectively. (a) The pump pulse arrives after the probe pulse, and excites the sample. This originates the anti-Stokes line since the outcoming frequency is higher than the one of the incoming pump fields. This is called IRS (I) process and (b) the probe pulse follows temporally the pump pulse and the Stokes line is generated because the outcoming frequency is smaller than the incoming one. This is the IRS (II) process.

According to Lee's papers [3, 14], it is possible to extrapolate the mathematical expression of the third-order polarization from the FDTL diagrams. The time-dependent third-order polarization in the IRS effect in the probe direction (i.e., wave vector $\boldsymbol{k}_{pr}$, is given by the overlap of the wave packet on the ket side of the time line and a ground vibrational state on the bra side. It depends on the transition dipole moment μ_{ge} on the inhomogeneous broadening of the wave packet $G(t)$ and it is integrated over the time intervals $t, \tau_1, \tau_2,$ and τ_3 :

$$P_{IRS(I)}^{(3)}(t)=\left(\frac{i}{\hbar}\right)^3\int_0^t d\tau_1\int_0^{\tau_1}d\tau_2\int_0^{\tau_2}d\tau_3 \times exp\left[-\frac{\gamma_g t}{2\hbar}-\frac{\gamma_e(t-\tau_1)}{2\hbar}-\frac{\gamma_d(\tau_1-\tau_2)}{\hbar}-\frac{\gamma_g(\tau_1-\tau_2)}{2\hbar}-\frac{\gamma_e(\tau_2-\tau_3)}{2\hbar}-\frac{\gamma_g\tau_3}{2\hbar}\right] \times E_{pu}(\tau_1)E_{pu}^*(\tau_2)E_{pr}(\tau_3)G(t-\tau_1+\tau_2-\tau_3)I(t,\tau_1,\tau_2,\tau_3) \tag{13}$$

$$P_{IRS(II)}^{(3)}(t)=\left(\frac{i}{\hbar}\right)^3\int_0^t d\tau_1\int_0^{\tau_1}d\tau_2\int_0^{\tau_2}d\tau_3 \times exp\left[-\frac{\gamma_g t}{2\hbar}-\frac{\gamma_e(t-\tau_1)}{2\hbar}-\frac{\gamma_d(\tau_1-\tau_2)}{\hbar}-\frac{\gamma_g(\tau_1-\tau_2)}{2\hbar}-\frac{\gamma_e(\tau_2-\tau_3)}{2\hbar}-\frac{\gamma_g\tau_3}{2\hbar}\right] \times E_{pr}(\tau_1)E_{pu}^*(\tau_2)E_{pu}(\tau_3)G(t-\tau_1+\tau_2-\tau_3)I(t,\tau_1,\tau_2,\tau_3) \tag{14}$$

Here, the four-time correlation function $I(t,\tau_1,\tau_2,\tau_3)$ is defined as follows:

$$I(t,\tau_1,\tau_2,\tau_3) = \left\langle \Psi_{g0}(\boldsymbol{Q})|e^{i\boldsymbol{h}_g/\hbar}\mu_{ge}e^{i\boldsymbol{h}_e(t-\tau_1)/\hbar}\times\mu_{eg}e^{i\boldsymbol{h}_g(\tau_1-\tau_2)/\hbar}\mu_{ge}e^{i\boldsymbol{h}_e(\tau_2-\tau_3)/\hbar}\times\mu_{eg}e^{i\boldsymbol{h}_g\tau_3/\hbar}|\Psi_{g0}(\boldsymbol{Q})\right\rangle \tag{15}$$

where $\boldsymbol{Q}$ is the multidimensional vibrational coordinate, $|\Psi_{g0}(\boldsymbol{Q})\rangle$ the initial ground vibrational state of the electronic ground state $|g\rangle$, and $\boldsymbol{h}_g$ and $\boldsymbol{h}_e$ the vibrational multidimensional Hamiltonians associated to the energetic levels involved in the transition $|g\rangle$ and $|e\rangle$ The terms γ_g and γ_e in Eqs. (13) and (14) are the line bandwidths of the two energetic levels, while γ_d is the time interval between τ_2 and τ_1, during which the vibrational coherence is lost (Raman vibrational dephasing time) [3].

Once defined the third-order polarization for both effects IRS (I) and IRS (II), it is possible to show the variation in intensity of the stimulated Raman signal as function of the frequencies, to be given by

$$\Delta I_{IRS}(\omega) = -\frac{8\pi^2 lC}{3n}\omega\,\Im\left\{E_{pr}^*(\omega)P_{IRS}^{(3)}(\omega)\right\} \tag{16}$$

where l is the optical path length, C the number of molecules per unit volume, and n the refractive index of the Raman-active medium. $E_{\mathrm{pr}}^*(\omega)$ is the incoming probe field with frequency ω and $P_{\mathrm{IRS}}^{(3)}(\omega)$ is the Fourier transform of the third-order polarization calculated using Eqs. (13) and (14). The variation in intensity $\Delta I_{\mathrm{IRS}}(\omega)$ is directly depending on the imaginary

http://dx.doi.org/10.5772/65479

part of the third-order Raman polarization, and hence on the Raman susceptibility as already stated in the previous section [15]. $\Im\left\{\chi^{(3)}(\omega)\right\}$ is negative at the Stokes frequencies ($\omega_S = \omega_L - \omega_v$) and positive at anti-Stokes frequencies ($\omega_{aS} = \omega_L + \omega_v$), as depicted in **Figure 3**, where the relation between the Stokes and anti-Stokes susceptibilities is presented. It follows that the Raman spectrum will be positive at the Stokes frequencies, experiencing a gain in the probe-beam intensity for each frequency which fulfills $\omega_S = \omega_L - \omega_v$. On the contrary, $\Delta I_{\mathrm{IRS}}(\omega) < 0$ in the anti-Stokes region. Here, the probe-beam intensity will be decreased for all those frequencies which meet the condition $\omega_{aS} = \omega_L + \omega_v$.

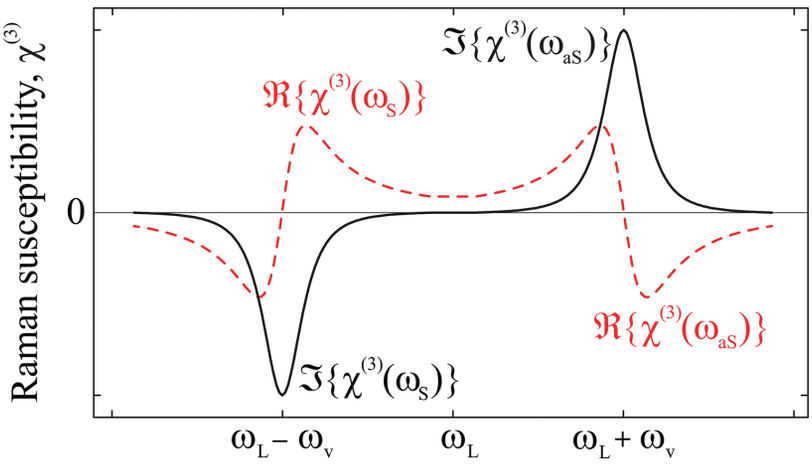

Figure 3. Relation between the Stokes and anti-Stokes susceptibilities. The solid black line is the imaginary part of the Raman susceptibility; the red dashed line is the real part of the Raman susceptibility.

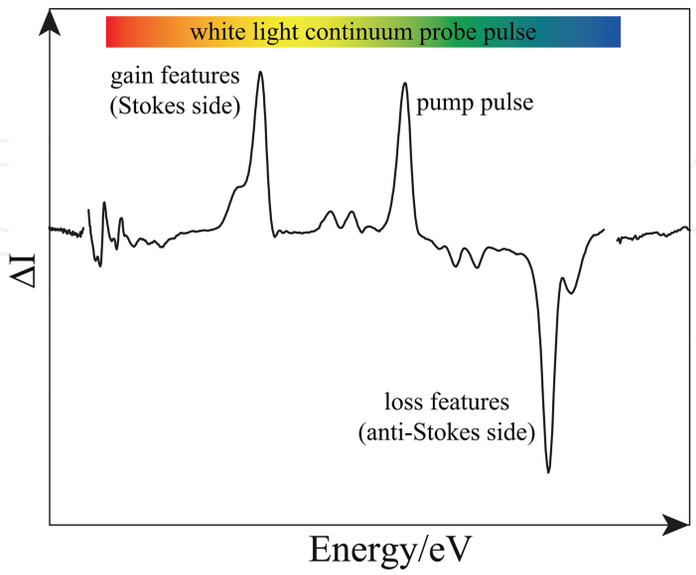

Figure 4. Extracted Raman spectrum of eumelanin dispersion in DMSO-methanol mixture.

The aforementioned variation in intensity $\Delta I_{\mathrm{IRS}}(\omega)$ will be analyzed for a case of study of a dispersion of eumelanin in dimethyl sulfoxide DMSO-methanol mixture (1:20 ratio) in the following. In **Figure 4**, the extracted Raman spectrum of the dispersion is depicted. On the red side of the white-light broadband spectrum (Stokes side), some frequencies resonate with the vibrational modes of the Raman-active medium. Hence, the signal appears as gain features in the probe pulse at those specific frequencies. At the same time, on the blue side (anti-Stokes side) a loss in the intensity is achieved at frequencies $\omega_{aS} = \omega_{pu} + \omega_{v}$.

4. Inverse Raman scattering: experiments

4.1. Experimental setup

To carry out FTA measurements, a noncollinear geometry in the pump-probe setup is used. A diode-pumped Ti:Sapphire femtosecond oscillator generates a ~100 fs pulse at a repetition rate of 78 MHz. The so-generated pulses are stretched and amplified by a regenerative Ti:Sapphire amplifier, pumped by a Q-switched Nd^{3+}:YLF laser at 1-KHz repetition rate, and eventually compressed, leading to 4 mJ, ~100 fs pulses at 798 nm. A beam splitter sends 90% of the outcoming pulse to an optical parametric amplifier to provide tunability over a broad spectral range (290–2600 nm). This tuneable laser pulse is sent through a depolarizer, an optical chopper, and finally focused on the sample in 1 mm spot, yielding an excitation density of 5×10^{14} photon pulse^{-1} cm^{-2}. The remaining 10% of the radiation is delayed in time by an optical delay line and focused on a CaF_2 crystal to generate a white-light continuum radiation, spanning between 450 and 800 nm. The WLC radiation is used as probe beam spatially overlapped to the pump pulse on the sample. The light transmitted by the sample is coupled into an optical fiber and sent to a charge-coupled device (CCD) spectrometer. The temporal resolution (~200 fs) is determined by the cross-correlation between the width of pump and probe pulses overlapping on the sample. The chromatic aberrations are removed by chirp correction software.

4.2. The IRS related to FTA experiments

So far, the nature of the IRS has been described. In this section, the IRS will be treated in relation with femtosecond transient absorption (FTA) experiments. In an FTA experiment, the intensity transmitted by an unexcited medium is given by $I_{\mathrm{pr}}^{0}(\hbar\omega)$, when the medium is excited by a pump pulse, a difference in the probe intensity is detected, and can be described as

$$\Delta I_{FTA}\left(\hbar\omega,\tau\right) = I_{pr}^{0}\left(\hbar\omega\right) - I_{pr}^{pu}\left(\hbar\omega,\tau\right), \tag{17}$$

where $I_{\mathrm{pr}}^{\mathrm{pu}}(\hbar\omega,\tau)$ is the probe intensity transmitted by the sample in the presence of the pump, and τ is the time delay between pump and probe pulses. Conversely, the variation in intensity

http://dx.doi.org/10.5772/65479

measured at the Stokes and anti-Stokes frequencies in the broadband spectrum of the probe pulse will be measured as the difference between the signal with and without the pump pulse: $I_{\text{pump-on}} - I_{\text{pump-off}}$ [16]. It results that

$$\Delta I_{IRS}(\omega,\tau) \propto -\Delta I_{FTA}(\hbar\omega,\tau). \tag{18}$$

By expressing the transient absorption signal as function of the detected difference in intensity, Eq. (19) can be obtained

$$\Delta A(\hbar\omega,\tau) = -\log_{10}\left[1-\frac{\Delta I_{FTA}(\hbar\omega,\tau)}{I^0_{pr}(\hbar\omega)}\right], \tag{19}$$

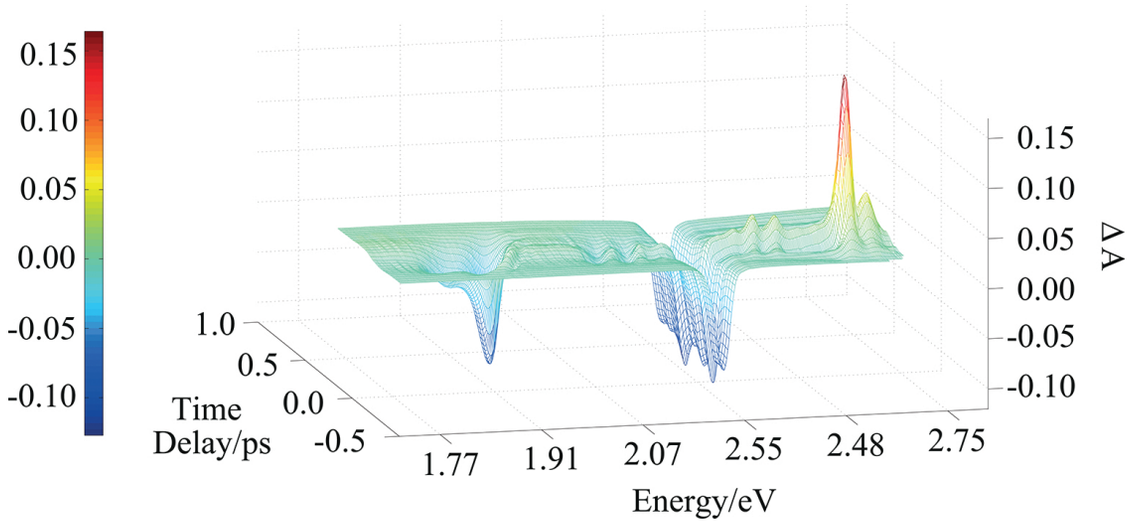

Figure 5. Three-dimensional plot of a femtosecond transient absorption experiment performed in eumelanin dispersed in a DMSO-methanol mixture. The sample was excited at 2.294 eV and probed over a range spanning from 1.548 to 2.753 eV. From left to right, the Stokes, laser pump, and anti-Stokes peaks can be identified. The $\Delta A(\hbar\omega,\tau)$ is shown in the first picosecond of time delay between the pump and probe pulses to clearly exhibit the Raman peaks.

and, thus, it is possible to directly relate the IRS effect to the FTA measurements. At Stokes frequencies, the probe-beam field experiences gain in intensity as already described above. Hence, the argument of the logarithm in Eq. (19) is larger than 1 and the transient absorption $\Delta A(\hbar\omega,\tau) < 0$. In fact, an increase in the photon flux is detected in the transmitted probe beam. Conversely, at anti-Stokes frequencies, a loss in intensity is experienced in the Raman-active medium, due to the annihilation of a photon of frequency ω_{aS}. Experimentally, the decrease in intensity in the transmitted probe beam can be treated as a real absorption by the sample, being $\Delta A(\hbar\omega,\tau) > 0$. This is precisely illustrated in **Figure 5**. In the middle, the scattered radiation from the incoming pump beam is evident. Symmetrically located with respect to the

pump laser, the upside-down peaks at low energies are the Stokes lines, while the intense peaks at high energies are the anti-Stokes lines.

Due to the different amount of photons detected in the femtosecond transient absorption experiments caused by the inverse Raman-scattering effect, it is crucial to recognize the presence of such coherent artifact to avoid misinterpretation in the analysis of the FTA spectra. Hereafter, the relaxation dynamics of a dispersion of eumelanin suspended in a DMSO-methanol mixture (1:20 ratio) is investigated by means of FTA. This sample was chosen to demonstrate the influence of the IRS, whose signal arises from the solvent used, in the temporal relaxation of the eumelanin pigments.

4.3. Decoupling IRS features from FTA dynamics

To investigate the influence of the IRS on the transient absorption dynamics, suitable probing energies have to be chosen accurately. To this end, the temporal evolutions of the Raman features have been analyzed. From **Figure 6**, it is clear that probing the sample dynamics at $\hbar\omega_{pr}$ = 1.741 eV allows the investigation of a region free from IRS features (probe frequency lower than the Stokes peaks, $\hbar\omega_{pr} < \hbar\omega_S$) . Furthermore, this is the energy at which the pigment is showing its maximum absorption, as illustrated in the inset of **Figure 6**. The other two regions where it is worth to investigate the dynamics are $\hbar\omega_{pr}$ = 1.823 and $\hbar\omega_{pr}$ = 2.460 eV. These two probing energies allow to study regions near the IRS features at energies lower (between the Stokes and the pump frequencies, $\hbar\omega_S < \hbar\omega_{pr} < \hbar\omega_{pu}$) and higher (between the pump and the anti-Stokes frequencies, $\hbar\omega_{pu} < \hbar\omega_{pr} < \hbar\omega_{aS}$) than the incoming pump pulse, respectively.

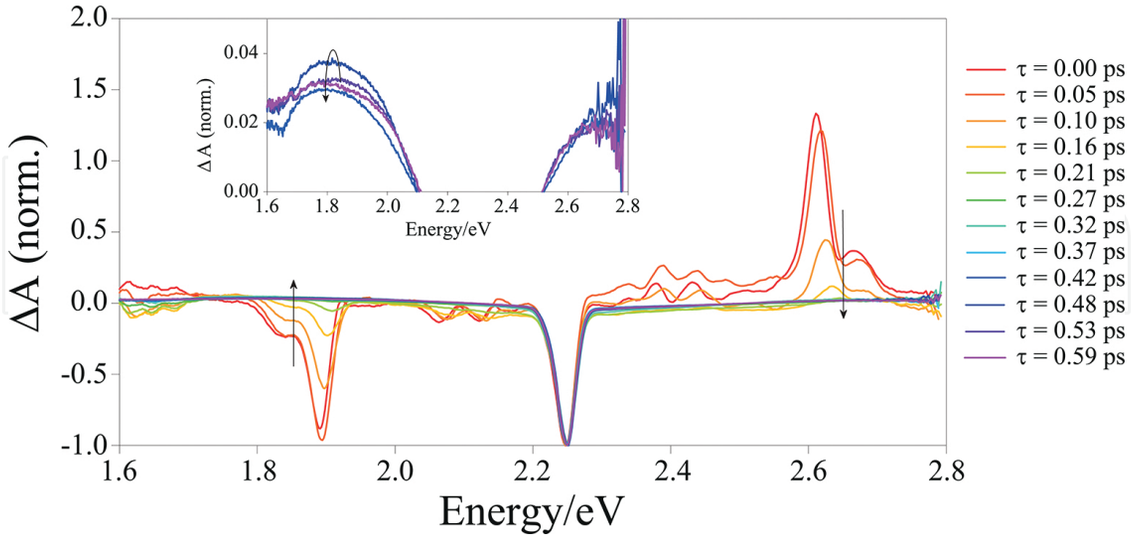

Figure 6. Temporal evolution of the synthetic eumelanin transient absorption spectra acquired in DMSO-methanol mixture after excitation at 2.254 eV. The spectra have been normalized to the pump-pulse intensity. The τ on the right illustrates the delay times between the pump and the probe pulses at which the spectra were acquired. The inset points out the rising of the eumelanin absorption signal, in an enlarged scale.

http://dx.doi.org/10.5772/65479

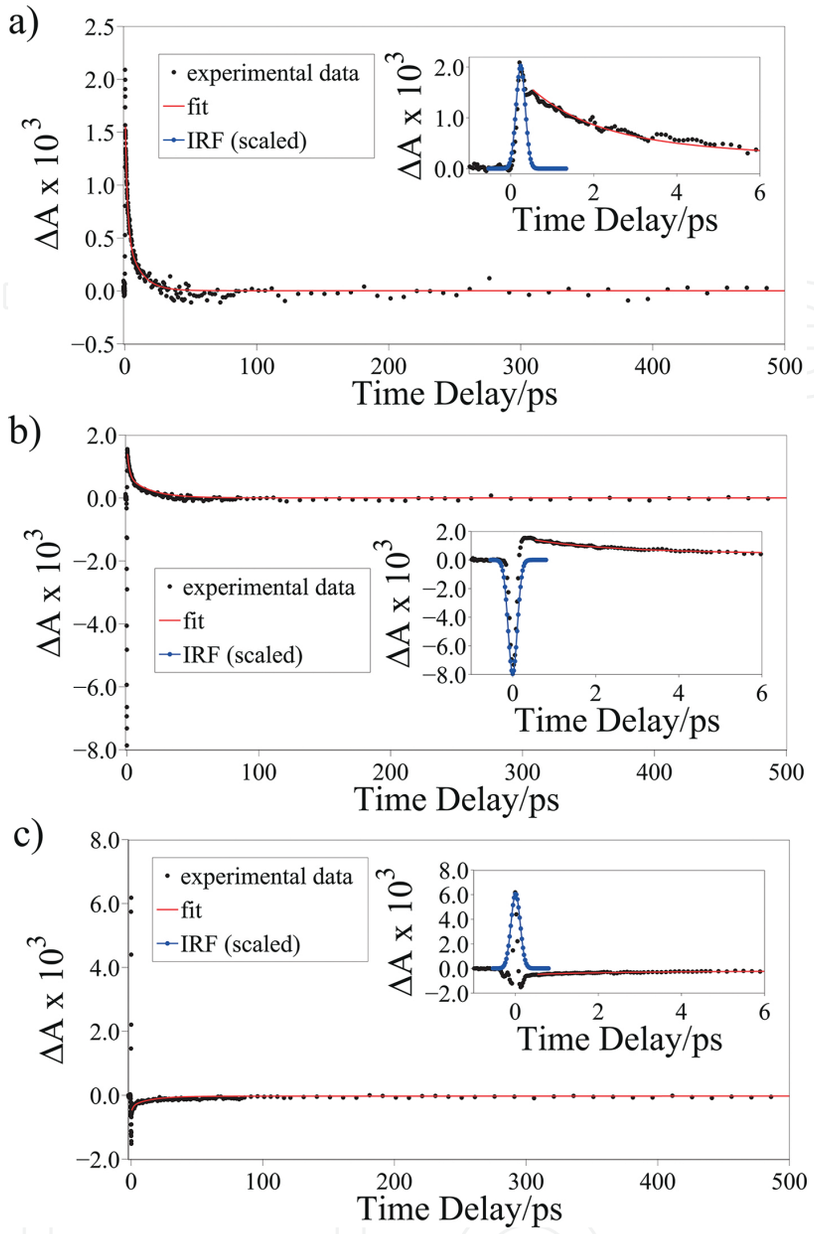

Figure 7. Transient absorption dynamics acquired in synthetic eumelanin dispersed in DMSO-methanol mixture. Dispersion has been excited at 2.254 eV and probed at energies $\hbar\omega_{\mathrm{pr}} < \hbar\omega_S$ (a), $\hbar\omega_S < \hbar\omega_{\mathrm{pr}} < \hbar\omega_{\mathrm{pu}}$ (b) and $\hbar\omega_{\mathrm{pu}} < \hbar\omega_{\mathrm{pr}} < \hbar\omega_{aS}$ (c), that is, 1.741, 1.823, and 2.460 eV, respectively. The experimental data (full circles) were fitted by a bi-exponential decay function (red solid line); the blue line shows the instrumental response function (IRF). Figure revised from [17].

The dynamics in the aforementioned regions is shown in **Figure 7** for the eumelanin suspension in DMSO-methanol mixture [17]. The temporal relaxation of these pigments is well reported [18], and is consistent with the data herein shown. At the same time, it is possible to appreciate a change in the sign of the differential absorption at very short time delays (first hundreds of femtoseconds) upon the probed energy, disclosing the influence of the IRS. When the probe-beam frequency is lower than the one at which the Stokes features appears, an IRS-free FTA

dynamics is observed. In fact, as presented in **Figure 7a** ($\hbar\omega_{pr}$ = 1.741 eV), the FTA dynamics shows a positive ΔA signal which decreases in time in a multi-exponential way. This signal is indicative of a photo-induced absorption, where the intensity of the transmitted probe beam in the presence of excitation by the pump pulse is lower than the one collected in the absence of the pump beam. In fact, upon excitation at $\hbar\omega_{pu}$ = 2.254 eV, an excited-state absorption (ESA) process, involving optically allowed transitions to higher-energy states, occurs in the eumelanin dispersion [19, 20]. When the response of the sample is probed at frequencies between the Stokes features and the incoming pump pulse, a profile like the one shown in **Figure 7b** is observed. Here, the dynamics is made out of a negative ΔA signal at ultrashort time delay followed by a sharp rise, ending by a bi-exponential decay. The observed signal is a convolution of two processes: the absorption of the pigments and the IRS effect arising from the solvent. As observed in the previous case, the eumelanin absorption leads to a positive ΔA signal at every time delay between pump and probe pulses.

The second contribution occurs only in the first hundreds of femtoseconds instead. This is due to the fact that the vibrational coherence needed to achieve the inverse Raman scattering persists as long as pump and probe pulses are temporally overlapped. Since the frequency of the probe pulse resonates with one of the Stokes features, a reinforcement of the vibrational modes of the solvent follows. Due to the resonance at the Stokes frequency, a gain in the intensity of the probe beam is achieved and the IRS appears as an emission of photons as described by the theoretical model presented by Rai et al. [4]. An increase in transmitted intensity is registered as a negative ΔA signal in an FTA experiment. Being a stimulated process, the IRS intensity overwhelms the absorption signal carried by the eumelanin pigments until the vibrational coherence lasts. When the delay between pump and probe pulses increases, the IRS artifact disappears, revealing the positive absorption of the eumelanin. Right after, the suspension relaxes back to the ground state following a bi-exponential decay.

In **Figure 7c**, the FTA dynamics of the eumelanin probed at frequencies between the incoming pump beam and the anti-Stokes features is presented. If $\hbar\omega_{pu} < \hbar\omega_{pr}$, a depletion of the ground state is achieved through the action of the pump pulse. This process is called ground-state bleaching and results in a negative ΔA signal, since the transmitted intensity of the probe beam is higher when the sample is excited. However, the ground-state bleaching cannot explain the presence of a sharp and intense positive peak in the first few hundreds of femtoseconds of the dynamics. Again, the IRS effect plays a major role at ultrashort delay times. In fact, the resonance between the incoming fields and the vibrational modes of the solvent occurring this time at the anti-Stokes frequencies leads to the stimulated Raman process. The loss in intensity experienced by the probe pulse can be accounted for as additional absorption, described by a positive ΔA signal. When the pump and probe pulse are no more overlapped in the sample, the phase-matching condition for the IRS is not satisfied, and the eumelanin dynamics is disclosed, recovering the signal in a bi-exponential fashion.

The decay time obtained from the fit of the eumelanin dynamics is reported in **Table 1** for the DMSO-methanol suspension. It is worth noting that regardless of the frequency of the probe pulse, the decay times of the samples are comparable. In fact, the IRS does not affect the

http://dx.doi.org/10.5772/65479

relaxation dynamics of the pigment. However, the IRS influences the sign and the amplitude of the FTA measurements.

Solvent	Probe energy (eV)	τ_1 (ps)	τ_2 (ps)
DMSO-methanol	1.741	1.5 ± 0.2	10.1 ± 0.9
	1.823	1.6 ± 0.3	16.9 ± 1.4
	2.460	1.5 ± 0.1	15.3 ± 1.2

Table 1. Fitting decay time values of eumelanin suspensions, carried out in DMSO-methanol mixture. The suspension was excited at 2.254 eV. Table adapted from [17].

4.4. Ultrafast Raman loss spectroscopy as diagnostic tool

The very need of high spatial and temporal resolution to investigate molecular reaction pathways has pushed toward the development of femtosecond stimulated Raman scattering. The aim is to be able to follow structural changes in molecules during a reaction occurring on short timescales, spanning from femtoseconds to picoseconds. The ability of femtosecond stimulated Raman spectroscopy lies in the high temporal resolution with which molecular vibrations can be collected, giving deep insights into reaction dynamics. Charge-transfer processes have been intensely investigated by FSRS; for example, long-debated studies on 4-(dimethylamino)benzonitrile, due to the discrepancy between the structural simplicity of this push-pull molecule and the complexity of the excited electronic levels, have been recently come to an end. In fact, the crucial role played by intramolecular and solvent reorganizations has been at the forefront of a systematic investigation, regarding three different dynamics on various timescales: the $\pi\pi^*$ relaxation, the internal conversion, and the vibrational relaxation [21, 22]. By investigating the excited-state proton transfer by FSRS, Fang et al. attributed to the skeletal motions the origin of the fluorescent form of a green fluorescent protein from *Aequorea victoria*, which is famous for its efficient bioluminescence [23]. Indeed, by looking separately at the low vibrational frequencies of specific modes, it was possible to identify an out-of-phase motion of the phenoxil ring in the chromophore, and thus to optimize the chemical structure of the chromophore for improving the excited-state proton transfer. Another important role in which FSRS is actively utilized is to help reveal the role that molecular symmetry plays in vibrational coherence activity in photosynthetic systems (as carotenoids) and in photochemistry. In particular, internal conversion processes and coupling between electronic states are ruled out [24, 25]. Finally, the vast majority of chemical reactions studied by FSRS concerns the isomerization, because of its key function in chromophores of high significance in biology. For example, Kuramochi et al. presented the first information pertaining to the vibrations in early instants of the photodynamics observed in the chromophore of the photoactive yellow protein. This study provided more insights on how to trigger the photoreceptive functions of the chromophore when embedded in the protein [26]. Kukura et al., instead, explored the spectral evolution of specific vibrational modes explaining how the activation of rhodopsin, a light

receptor, is driven by geometric changes in the retinal backbone [27]. These are just few of the large number of examples that can be recalled to demonstrate the power of FSRS to unravel reaction coordinates, chemical configurations, and nuclear dynamics.

One of the specific methods enrolled by the femtosecond-stimulated Raman spectroscopy relies on the IRS effect and is called femtosecond inverse Raman scattering (FIRS) [2], or ultrafast Raman loss spectroscopy (URLS) [4]. In URLS, the decrease in intensity of the probe beam, as described in Section 4.2, is completely described by the IRS effect and is used as fingerprint to follow in time the reaction pathways. Moreover, this spectroscopic tool shows some beneficial features missing in the general FSRS. The intensity of the Raman peaks at the anti-Stokes frequencies results higher than what is measured at the Stokes frequencies (Raman gain), leading to a better signal-to-noise ratio [7, 9, 10]. Second, looking at the blue side of the pump pulse to identify the spectral features of the sample helps to reject the fluorescence signal, which appears on the red side [2]. Finally, the detector dynamic range has higher efficiencies on the anti-Stokes than on the Stokes side, minimizing the noise levels and thus allowing for clearer imaging (FIRS microscopy) [28–32], for example, in tissues [33] and drug-delivery processes [34–36].

In the previous paragraph, it was shown that investigating the temporal evolution of the ΔA signal at specific probing energies can be used to determine the influence of the IRS coherent artifact on the dynamics of the eumelanin pigments. Focusing now on the IRS features, the dynamics of specific bonds, induced by photoexcitation processes, can be probed [37, 38].

First, it is of crucial importance to identify the spectral features encountered in the FTA measurements, and ascribe them to specific vibrational modes. To this end, the Raman spectrum of the solvent mixture (DMSO-methanol, 1:20 in ratio) was collected. As can be seen in **Figure 8a**, the Raman spectrum is dominated by three narrow peaks and a broad band. These features are recognized as follows: CO stretching and SO stretching in methanol and in DMSO, overlapping at 0.125 eV (peak I); CH_2 bending in methanol at 0.177 eV (peak II); CH stretching in methanol at 0.352 and 0.365 eV (symmetric and antisymmetric vibrational mode), and in DMSO at 0.361 eV (peak III); OH stretching in methanol at 0.414 eV (peak IV) [39–41]. A direct correspondence of the Raman peaks shown in **Figure 8a** is found in the FTA measurements depicted in **Figure 8b**. In fact, the spectral evolution at ultrashort time delays shows specifically the same Raman features occurring symmetrically to the pump pulse at Stokes and anti-Stokes frequencies.

Tuning the pump pulse to lower energies, the spectral features follow the energy shift, maintaining constant the energy difference between each of them and the pump pulse (spectra from red to blue in **Figure 8b**). Computing $\Delta E = \hbar\omega_{\mathrm{pu}} - \hbar\omega_i$, that is, the difference in energy between the pump pulse and the spectral features, this equals the Raman shift values displayed on the x-axes for each Raman peak reported in **Figure 8a**. By this analysis, the authors proved that the observed coherent artifact in the FTA measurements at ultrashort time delay is a feature originating from the stimulated Raman-scattering process [17].

http://dx.doi.org/10.5772/65479

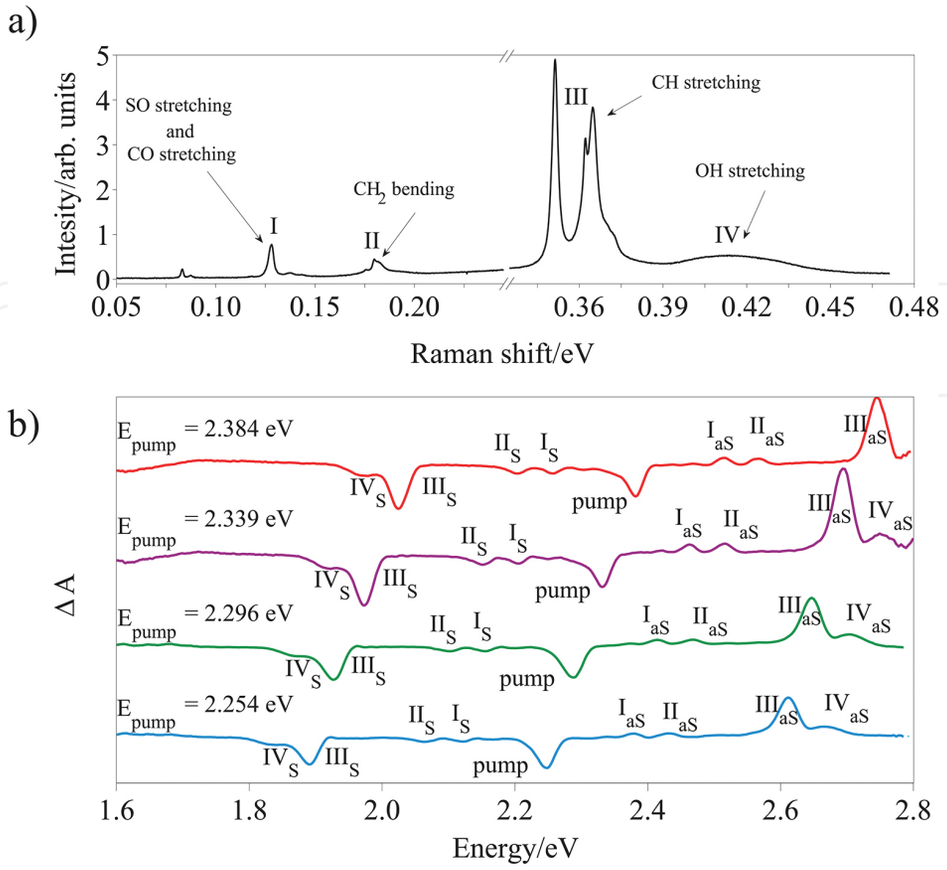

Figure 8. (a) Raman spectrum of DMSO-methanol mixture (λ_{ex} = 488 nm, $P_{incident}$ = 6 mW, acquisition time: 30 s) and (b) Spectral evolution of the transient absorption signal detected at $\tau \sim 0$ in the DMSO-methanol mixture for different pump-pulse energies. The curves are vertically shifted for clarity. Figure taken from [17].

Once identified the Raman vibrational modes, it is possible by URLS to investigate them specifically and, in particular, to address their spectral evolution in time. This can give insights on the transient structure of the molecules and on the dynamics of the specific vibrational modes. Here, we report on a very preliminary analysis ran in such direction on the aforementioned sample; in **Figure 9** the C—H Raman vibrational mode located at 2.641 eV, upon pumping the sample at $\hbar\omega_{pu}$ = 2.525 eV, is examined in terms of peak shift and intensity over time. The spectra shown in **Figure 9a** have been normalized to the intensity of the incoming pump pulse. The peak position experiences a shift toward the blue region of the spectrum as the temporal decoupling of pump and probe pulses occurs. This can be clearly seen in **Figure 9b** within the first picoseconds. At the same time, its intensity decreases at an exponential rate (**Figure 9c**).

This example should visually explain the potential and the strength of the URLS as spectroscopic tool. In fact, the results here collected, and the many more presented in literature [37, 38, 42], unambiguously demonstrate the ability of the technique to select specific bonds and study their dynamics upon photoexcitation, at ultrafast timescales. However, further investigations are required to relate the experimental observations to the ultimate structure of the solvent molecules.

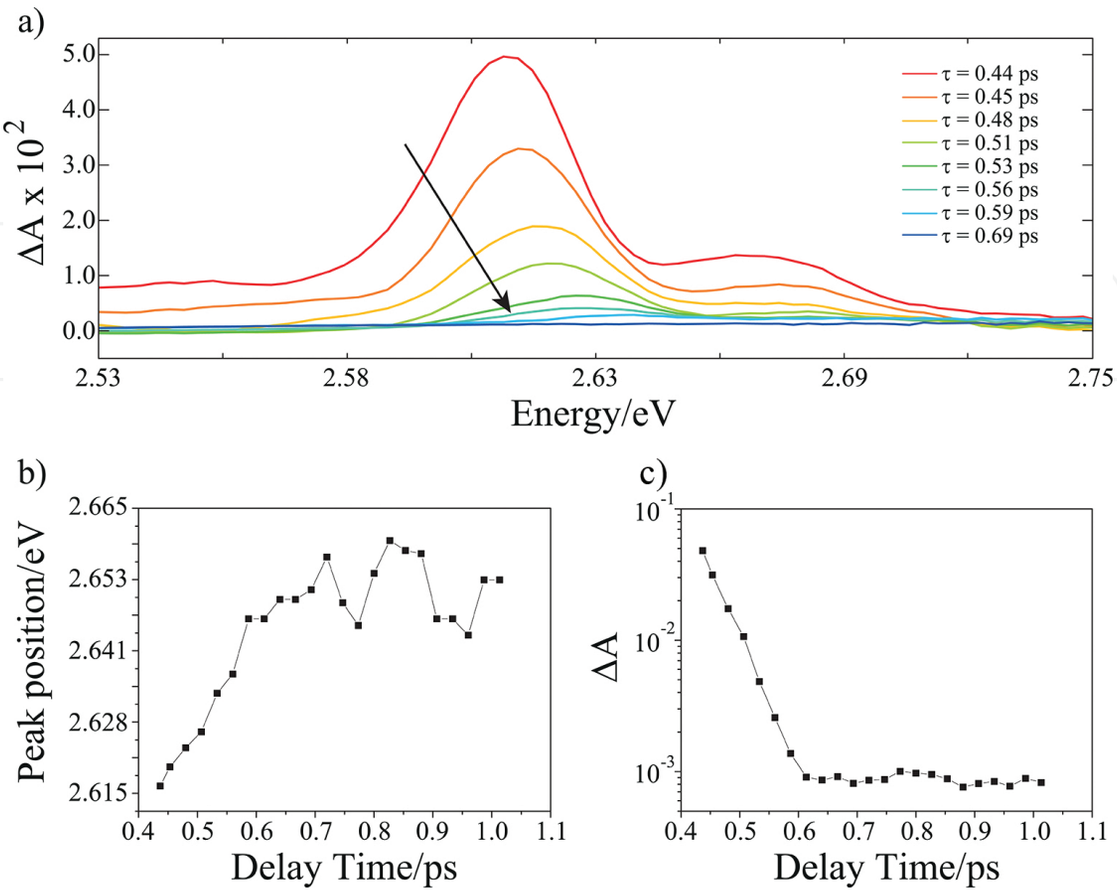

Figure 9. (a) ΔA signal in the blue region of the pump pulse. The peak taken into account is the anti-Stokes feature related to the stretching of the C—H bond in methanol and DMSO, (b) evolution of the Raman peak position as function of delay time between the pump and the probe pulses, and (c) temporal evolution of the intensity of the Raman peak.

5. Conclusions

In this chapter, the authors presented a complete description of the inverse Raman scattering effect, one of the four-wave mixing processes contributing to the stimulated Raman scattering process. Feynman dual-time line diagrams and energy level diagrams were used to explain the theory behind the IRS effect. Once addressed the nature of the IRS effect, its close relation with the transient absorption pump-probe experiment was described, as well as the influence on the temporal evolution of the sample dynamics. To this end, the dynamics of eumelanin dispersions carried out at different exciting energies were shown, pointing out the crucial role of the IRS in the relaxation dynamics of the sample. Finally, the implementation of the IRS effect as diagnostic tool in determining the structures and interactions among molecules was presented. In fact, the high resolution achieved in the time and spectral domains showed by ultrafast loss Raman spectroscopy enables to follow specifically the electronic structure of molecules while undergoing chemical reactions, even on ultrafast timescales.

Author details

Antonio Aloi[1,2] and Raffaele Tommasi[3,4*]

*Address all correspondence to: raffaele.tommasi@uniba.it

1 Institute for Complex Molecular Systems (ICMS), Eindhoven University of Technology, Eindhoven, Netherlands

2 Laboratory of Macromolecular and Organic Chemistry, Department of Chemical Engineering and Chemistry, Eindhoven University of Technology, Eindhoven, Netherlands

3 Department of Basic Medical Sciences, Neuroscience and Sense Organs, University of Bari Aldo Moro, Bari, Italy

4 CNR-IPCF Bari Divison, c/o Chemistry Department, Bari, Italy

References

[1] Wei, J. Nonlinear Super-Resolution Nano-Optics and Applications. 1st ed. Springer-Verlag Berlin Heidelberg; 2015. DOI: 10.1007/978-3-662-44488-7.

[2] Dietze, D.R.; Mathies, R.A. Femtosecond stimulated Raman spectroscopy. Chem. Phys. Chem. 2016; 17:1–29. DOI: 10.1002/cphc.201600331

[3] Qiu, X.; Li, X.; Niu, K.; Lee, S.Y. Inverse Raman bands in ultrafast Raman loss spectroscopy. J. Chem. Phys. 2011; 135:164502-1-8. DOI: 10.1063/1.3653940.

[4] Rai, N.K.; Lakshmanna, A.Y.; Namboodiri, V.V.; Umapathy, S. Basic principles of ultrafast Raman loss spectroscopy. J. Chem. Sci. 2012; 124:177–186. DOI: 10.1007/s12039-012-0214-8.

[5] Jones, W.J.; Sticheff, B.P. Inverse Raman spectra: induced absorption at optical frequencies. Phys. Rev. Lett. 1964; 13:657–660. DOI: 10.1103/PhysRevLett.13.657.

[6] Roslyak, O.; Marx, C.A.; Mukamel, S. Generalized Kramers-Heisenberg expressions for stimulated Raman scattering and two-photon absorption. Phys. Rev. A. 2009; 79:063927-1-12. DOI: 10.1103/PhysRevA.79.063827.

[7] Mallick, B.; Lakhsmanna, A.Y.; Umapathy, S. Ultrafast Raman loss spectroscopy (URLS): instrumentation and principles. J. Raman Spectrosc. 2011; 42:1883–1890. DOI: 10.1002/jrs.2996.

[8] Lau, A.; Werncke, W.; Pfeiffer, M.; Lenz, K.; Weigmann, H.J. Inverse Raman scattering. Sov. J. Quant. Electron. 1976; 6:402–409. DOI: 10.1070/QE1976v006n04ABEH011129/meta.

[9] Umapathy, S.; Lakhsmanna, A.Y.; Mallick, B. Ultrafast Raman spectroscopy. J. Raman Spectrosc. 2009; 40:235–237. DOI: 10.1002/jrs.2199.

[10] Lakhsmanna, A.Y.; Mallick, B.; Umapathy, S. Ultrafast Raman loss spectroscopy: a new approach to vibrational structure determination. Curr. Sci. 2009; 97:210–216.

[11] Abramczyk, H. Introduction to laser spectroscopy. 1st. ed. Elsevier; Radarweg 29, P.O. Box 211, 1000 AE Amsterdam, The Netherlands; 2005. DOI: 9780444516626.

[12] Niu, K.; Lee, S.Y. Analysis of time resolved femtosecond and femtosecond/picosecond coherent anti-Stokes Raman spectroscopy: Application to toluene and Rhodamine 6G. J. Chem. Phys. 2012; 136:064504-1-11. DOI: 10.1063/1.3682470.

[13] Frontiera, R.R.; Shim, S.; Mathies, R.A. Origin of negative and dispersive features in anti-Stokes and resonance femtosecond stimulated Raman spectroscopy. J. Chem. Phys. 2008; 129:064507-1-6. DOI: 10.1063/1.2966361.

[14] Niu, K.; Cong, S.; Lee, S.Y. Femtosecond stimulated Raman scattering for polyatomics with harmonic potentials: application to rhodamine 6G. J. Chem. Phys. 2009; 131:054311-1-14. DOI: 10.1063/1.3198473.

[15] Boyd, R. Nonlinear Optics. 3rd. ed. Academic Press; 30 Corporate Drive, Suite 400, Burlington, MA 01803, USA, 525 B Street, Suite 1900, San Diego, California 92101-4495, USA, 84 Theobald's Road, London WC1X 8RR, UK; 2008. DOI: 9780123694706.

[16] Sun, Z.; Lu, J.; Zhang, D.H.; Lee, S.Y. Quantum theory of (femtosecond) time-resolved stimulated Raman scattering. J. Chem. Phys. 2008; 128:144114-1-13. DOI: 10.1063/1.2888551.

[17] Aloi, A.; Brunetti, A.; Perna, G.; Lasalvia, M.; Capozzi, V.; Tommasi, R. Ultrafast transient absorption of eumelanin suspensions: the role of inverse Raman scattering. Biomed. Opt. Express. 2015; 6:4000–4013. DOI: 10.1364/BOE.6.004000.

[18] Matthews, T.E.; Wilson, J.W.; Degan, S.; Simpson, M.J.; Jin, J.Y.; Zhang, J.Y.; Warren, W.S. In vivo and ex vivo epi-mode pump-probe imaging of melanin and microvasculature. Biomed. Opt. Express. 2011; 2:1576–1583. DOI: 10.1364/BOE.2.001576.

[19] Berera, R.; van Grondelle, R.; Kennis, J.T.M. Ultrafast transient absorption spectroscopy: principles and application to photosynthetic systems. Photosynth. Res. 2009; 101:105–118. DOI: 10.1007/s11120-009-9454-y.

[20] Meredith, P.; Sarna, T. The physical and chemical properties of eumelanin. Pigment Cell Res. 2006; 19:572–594. DOI: 10.1111/j.1600-0749.2006.00345.x.

[21] Rhinehart, J.M.; Mehlenbacher, R.D.; McCamant, D.W. Probing the charge transfer reaction coordinate of 4-(Dimethylamino)benzonitrile with femtosecond stimulated Raman spectroscopy. J. Phys. Chem. B. 2010; 114:14646–14656. DOI: 10.1021/jp1023982.

[22] Rhinehart, J.M.; Challa, J.R.; McCamant, D.W. Multimode charge-transfer dynamics of 4-(Dimethylamino)benzonitrile probed with ultraviolet femtosecond stimulated Raman spectroscopy. J. Phys. Chem. B. 2012; 116:10522–10534. DOI: 10.1021/jp3020645.

[23] Fang, C.; Frontiera, R.R.; Tran, R.; Mathies, R.A. Mapping GFP structure evolution during proton transfer with femtosecond Raman spectroscopy. Nature. 2009; 462:200–205. DOI: 10.1038/nature08527.

[24] Hashimoto, H.; Sugisaki, M.; Yoshizawa, M. Ultrafast time-resolved vibrational spectroscopies of carotenoids in photosynthesis. Biochim. Biophys. Acta Bioenerg. 2015; 1847:69–78. DOI: 10.1016/j.bbabio.2014.09.001.

[25] Buckup, T.; Motzkus, M. Multidimensional time-resolved spectroscopy of vibrational coherence in biopolyenes. Annu. Rev. Phys. Chem. 2014; 65:39–57. DOI: 10.1146/annurev-physchem-040513-103619.

[26] Kuramochi, H.; Takeuchi, S.; Tahara, T. Ultrafast structural evolution of photoactive yellow protein chromophore revealed by ultraviolet resonance femtosecond stimulated Raman spectroscopy. J. Phys. Chem. Lett. 2012; 3:2025–2029. DOI: 10.1021/jz300542f.

[27] Kukura, P.; McCamant, D.W.; Yoon, S.; Wandschneider, D.B.; Mathies, R.A. Structural observation of the primary isomerization in vision with femtosecond-stimulated Raman. Science. 2005; 310:1006–1009. DOI: 10.1126/science.1118379.

[28] Robles, F.E.; Fischer, M.C.; Warren, W.S. Dispersion-based stimulated Raman scattering spectroscopy, holography, and optical coherence tomography. Opt. Express. 2016; 24:485–498. DOI: 10.1364/OE.24.000485.

[29] Puppels, G.J.; de Mul, F.F.; Otto, C.; Greve, J.; Robert-Nicoud, M.; Arndt-Jovin, D.J.; Jovin, T.M. Studying single living cells and chromosomes by confocal Raman microspectroscopy. Nature. 1990; 347:301–303. DOI: 10.1038/347301a0.

[30] Zumbusch, A.; Holtom, G.R.; Xie, X.S. Three-dimensional vibrational imaging by coherent anti-Stokes Raman scattering. Phys. Rev. Lett. 1999; 82:4142–4145. DOI: 10.1103/PhysRevLett.82.4142.

[31] Cui, M.; Bachler, B.R.; Ogilvie, J.P. Comparing coherent and spontaneous Raman scattering under biological imaging conditions. Opt. Lett. 2009; 34:773–775. DOI: 10.1364/OL.34.000773.

[32] Simpson, M.J.; Wilson, J.W.; Phipps, M.A.; Robles, F.E.; Selim, M.A.; Warren, W.S. Nonlinear microscopy of eumelanin and pheomelanin with subcellular resolution. J. Invest. Dermatol. 2013; 133:1822–1826. DOI: 10.1038/jid.2013.37.

[33] Ji, M.; Orringer, D.A.; Freudiger, C.W.; Ramkissoon, S.; Liu, X.; Lau, D.; Golby, A.J.; Norton, I.; Hayashi, M.; Agar, N.Y.R.; Young, G.S.; Spino, C.; Santagata, S.; Camelo-Piragua, S.; Ligon, K.L.; Sagher, O.; Xie, X.S. Rapid, label-free detection of brain tumors with stimulated Raman scattering microscopy. Sci. Transl. Med. 2013; 5:201ra119-1-10. DOI: 10.1126/scitranslmed.3005954.

[34] Fu, D.; Yu, Y.; Folick, A.; Currie, E.; Farese, R.V.Jr.; Tsai, T.-H.; Xie, X.S.; Wang, M.C. In vivo metabolic fingerprinting of neutral lipids with hyperspectral stimulated Raman scattering microscopy. J. Am. Chem. Soc. 2014; 136:8820–8828. DOI: 10.1021/ja504199s.

[35] Fu, D.; Zhou, J.; Zhu, W.S.; Manley, P.W.; Wang, Y.K.; Hood, T.; Wylie, A.; Xie, X.S. Imaging the intracellular distribution of tyrosine kinase inhibitors in living cells with quantitative hyperspectral stimulated Raman scattering. Nat. Chem. 2014; 6:614–622. DOI: 10.1038/nchem.1961.

[36] Tipping, W.J.; Lee, M.; Serrels, A.; Bruntonb, V.G.; Hulme, A.N. Stimulated Raman scattering microscopy: an emerging tool for drug discovery. Chem. Soc. Rev. 2016; 45:2075–2089. DOI: 10.1039/C5CS00693G.

[37] Umapathy, S.; Roy, K.; Kayal, S.; Rai, N.; Venkatraman, R.K. Structure and dynamics from time resolved absorption and Raman spectroscopy. Springer Netherlands; 2014. DOI: 10.1007/978-94-017-8550-1_3.

[38] Hoffman, D.P.; Mathies, R.A. Femtosecond stimulated Raman exposes the role of vibrational coherence in condensed-phase photoreactivity. Acc. Chem. Res. 2016; 49:616–625. DOI: 10.1021/acs.accounts.5b00508.

[39] Martens, W.N.; Frost, R.L.; Kristof, J.; Kloprogge, J.T. Raman spectroscopy of dimethyl sulphoxide and deuterated dimethyl sulphoxide at 298 and 77 K. J. Raman Spectrosc. 2002; 33:84–91. DOI: 10.1002/jrs.827.

[40] Cheng, J.X.; Xie, X.S. Coherent Raman scattering microscopy. CRC Press; Taylor & Francis Group, 6000 Broken Sound Parkway NW, Suite 300, Boca Raton, FL 33487-2742; 2012. DOI:9781439867655.

[41] Ellis, A.; Zehentbauer, F.M.; Kieferab, J. Probing the balance of attraction and repulsion in binary mixtures of dimethyl sulfoxide and n-alcohols. Phys. Chem. Chem. Phys. 2013; 15:1093–1096. DOI: 10.1039/C2CP42902K.

[42] Kukura, P.; McCamant, D.W.; Mathies, R.A. Femtosecond stimulated Raman spectroscopy. Annu. Rev. Phys. Chem. 2007; 58:461–488. DOI: 10.1146/annurev.physchem.58.032806.104456.